Crystal-plasticity finite-element simulation of time-dependent springback in a commercially-pure titanium sheet

Hama, T.; Sakai, T.; Korkolis, Y.P.; Takuda, H.

Journal of Physics: Conference Series

PAPER • **OPEN ACCESS**

Crystal-plasticity finite-element simulation of time-dependent springback in a commercially-pure titanium sheet

To cite this article: T. Hama *et al* 2018 *J. Phys.: Conf. Ser.* **1063** 012122

IOP Conf. Series: Journal of Physics: Conf. Series **1063** (2018) 012122 doi:10.1088/1742-6596/1063/1/012122

Crystal-plasticity finite-element simulation of time-dependent springback in a commercially-pure titanium sheet

T. Hama[1], T. Sakai[1], Y.P. Korkolis[2], and H. Takuda[1]

[1]Department of Energy Science and Technology, Kyoto University, Yoshida-honmachi, Sakyo-ku, Kyoto 606-8501, Japan
[2]Department of Mechanical Engineering and CAMMI – Center for Advanced Materials and Manufacturing Innovation, University of New Hampshire, 33 Academic Way, Durham, NH, 03824, USA

E-mail: hama@energy.kyoto-u.ac.jp

Abstract. A crystal-plasticity finite-element method was used to examine the deformation mechanism of time-dependent springback in a commercially-pure titanium sheet. To reproduce the viscoplastic behavior of the sheet, the material parameters were calibrated to reproduce the strain-rate dependency of the stress-strain curve under uniaxial tension. A two-dimensional draw bending process was simulated and the change in the sidewall curvature was evaluated. The simulation results showed that the curvature increased with the elapsed time after unloading, consistent with experimental results reported elsewhere. The deformation mechanism during the process was discussed in terms of evolution of stress and relative activities of slip and twinning systems.

1. Introduction

Commercially-pure titanium (CP-Ti) sheets are widely used in industrial products because of their characteristics such as high specific strength and corrosion resistance. Because CP-Ti sheets exhibit strongly anisotropic deformation behavior due to their hexagonal-close-packed (hcp) structure and strong basal texture, their deformation behaviors have been extensively studied from both macroscopic and microscopic viewpoints [1-10].

It was reported that some metallic sheets exhibit the so-called time-dependent springback at room temperature. Wang et al. [11] reported that in an aluminum sheet the amount of springback gradually increases with the elapsed time after unloading. Similar behavior was also observed in magnesium alloy and advanced high-strength steel sheets [12,13]. Hereafter this phenomenon is called elapsed time-dependent springback. Kyuno et al. [14] conducted a draw-bending test using a steel sheet and showed that the amount of springback decreased as the holding time before unloading increased. This phenomenon is hereafter called holding time-dependent springback. The holding and elapsed time-dependent springback were considered to result respectively from stress relaxation that occurs during holding and from creep driven by residual stresses after unloading [11-13,18]. Because it has been recognized that CP-Ti sheets show pronounced viscoplastic deformation behavior at room temperature [15-17], we examined time-dependent springback of a CP-Ti sheet experimentally [18] and found that a CP-Ti sheet also showed pronounced holding and elapsed time-dependent springback. Although the

deformation mechanism was discussed with respect to stress relaxation and creep [18], the discussion was only phenomenological and qualitative; thus, the detailed mechanism is still open to discussion.

In this study, a crystal plasticity finite-element method is used to examine elapsed time-dependent springback of a CP-Ti sheet. A two-dimensional draw bending process is simulated by using a crystal plasticity finite-element method, and the deformation mechanism at the mesoscopic level is discussed.

2. Crystal plasticity model

The crystal plasticity finite-element method used in our previous studies [3,19,20] was used. To model the viscoplastic deformation behavior of a CP-Ti sheet, the following viscoplastic power law was used to describe the slip rate $\dot{\gamma}^{\alpha}$ of the α slip system

$$\frac{\dot{\gamma}^{\alpha}}{\dot{\gamma}_0}=\left|\frac{\tau^{\alpha}}{\tau_{\mathrm{Y}}^{\alpha}}\right|^{\frac{1}{m}}\operatorname{sign}\left(\tau^{\alpha}\right),\quad \dot{\tau}_{\mathrm{Y}}^{\alpha}=\sum_{\beta}q_{\alpha\beta}h\left|\dot{\gamma}^{\beta}\right|, \tag{1}$$

where τ^{α} and $\tau_{\mathrm{Y}}^{\alpha}$ are the resolved shear stress and the current strength of the α slip system, respectively. $\dot{\gamma}_0$ is the reference strain rate, m is the rate sensitivity exponent and $q_{\alpha\beta}$ is the self ($\alpha=\beta$) and latent ($\alpha\neq\beta$) hardening moduli. The following two equations were used for the hardening rate h

$$h=h_0 \text{ and } h=h_0\left(1-\frac{\tau_0}{\tau_\infty}\right)\exp\left(-\frac{h_0\bar{\gamma}}{\tau_\infty}\right) \text{ with } \bar{\gamma}=\sum_{\alpha}\int\left|\dot{\gamma}^{\alpha}\right|\mathrm{d}t\,. \tag{2}$$

To model the plastic deformation of a CP-Ti sheet, five families of slip systems, i.e., basal $\{0001\}\langle 11\bar{2}0\rangle$ slip, prismatic $\{10\bar{1}0\}\langle 11\bar{2}0\rangle$ slip, pyramidal $\{10\bar{1}1\}\langle 11\bar{2}0\rangle$ slip, pyramidal $\{11\bar{2}2\}\langle 11\bar{2}3\rangle$ slip (pyr $\langle a+c\rangle$-1 slip), and pyramidal $\{10\bar{1}1\}\langle 11\bar{2}3\rangle$ slip (pyr $\langle a+c\rangle$-2 slip), and two families of twinning systems, i.e., $\{10\bar{1}2\}$ tensile twinning and $\{11\bar{2}2\}$ compressive twinning, were taken into account. The linear hardening (the first equation in eq. (2)) and Voce hardening (the second equation in eq.(2)) were assumed respectively for the twinning and slip systems. A twinning and detwinning model proposed by the authors was employed. The abovementioned crystal plasticity model was incorporated into a static finite-element method with explicit time integration.

3. Simulation conditions

A rolled grade 1 CP-Ti sheet with a thickness of 1 mm was modeled. The hardening parameters were determined to fit the stress-strain curves under uniaxial tension with various strain rates in the rolling direction. The hardening parameters determined are shown in Table 1. To represent the difference in rate sensitivity between slip and twinning systems, the rate sensitivity exponent was set to 0.02 and 0.0035 respectively to the slip and twinning systems. The self-hardening moduli were set to unity, whereas the parameters determined in literature [3] were used for the latent-hardening moduli.

The forming conditions of the two-dimensional draw-bending process were determined on the basis of experimental conditions [18] as follows. The punch width was 40 mm. The punch and die shoulder radii were respectively 5 mm and 10 mm. The clearance between the die and the punch was 1.6 mm. Because the purpose of this study was not to predict accurately the amount of springback but rather to examine the underlying deformation mechanism of the time-dependent springback, the problem was simplified as follows: the gap between the die and the blank holder was set to 1.02 mm and kept constant during the process, and friction between the sheet and the tools was neglected. The tools were assumed to be rigid. To simplify the problem, only a half part in the longitudinal direction of the sheet specimen was modeled by using eight node solid elements with selective reduced integration, and the plane strain condition was

Table 1. Hardening parameters used in simulation (MPa).

	Basal	Prism	Pyr<a>	Pyr<a+c>−1	Pyr<a+c>−2	{10$\bar{1}$2}	{11$\bar{2}$2}
τ_0	160	64	74	200	195	167	217
τ_∞	200	180	210	372	363	–	–
h_0	1950	1050	580	2050	2050	350	350

assumed in the depth direction. The size of the sheet model was 110 mm, 1 mm, and 1 mm respectively in the longitudinal, depth, and thickness directions. The size of the mesh was 1 mm, 1 mm, and 0.5 mm respectively in the longitudinal, depth, and thickness directions. A result of Electron Back-Scatter Diffraction (EBSD) measurement was used to determine the initial crystallographic orientations assigned to the finite-element model, 20 crystal orientations were assigned to each integration point using the Taylor model. The numbers of elements through the thickness and crystal orientations assigned to each integration point denote that there were 80 grains through the thickness direction in the simulation, which was comparable to the material used in the experiment that had the average grain size of approximately 16 μm. On the other hand, in terms of finite-element simulation, the number of elements through the thickness direction might not be enough to quantitatively compare with experimental results. Appropriate numbers of crystal orientations and elements will be the focus of our future work.

The punch was displaced to a stroke of 50 mm with the velocity of 10 mm/min. After the punch stroke reached 50 mm, the tools were retracted to unload the sheet. After the sheet was macroscopically unloaded from the tools, an average of the curvatures at the sidewall was used to evaluate the amount of springback, as shown in Fig. 1 (a). Further, the change in the curvature as a function of elapsed time after unloading was measured.

4. Results and discussion

Figure 1 (b) shows the relationship between the curvature and the elapsed time after unloading. The curvature increased with the elapsed time. The increase in curvature from 5 min to 100 min was approximately 7 %. These results are in qualitatively good agreement with the experimental results of a grade 2 CP-Ti sheet [18] although the increasing rate was larger in the simulation. It should be noted

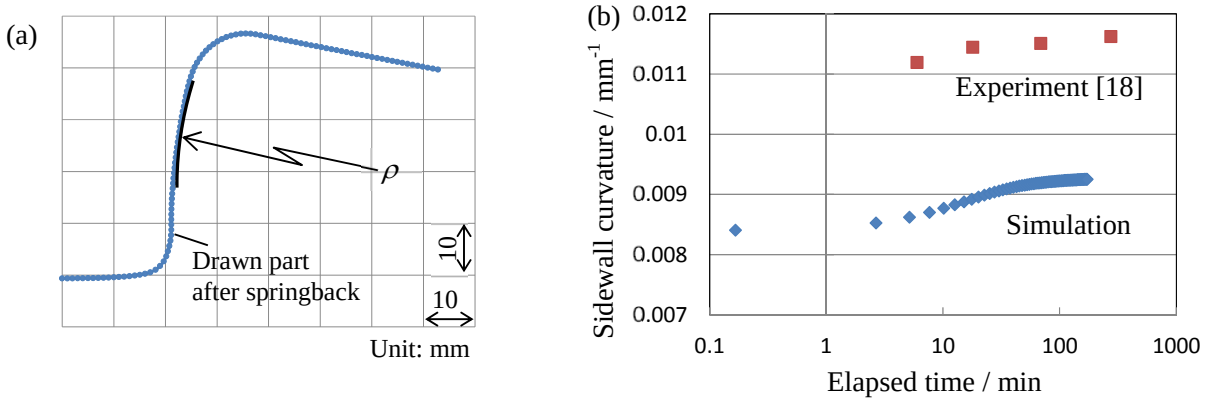

Figure 1. Simulation results of springback. (a) Schematic drawing of curvature at the sidewall and (b) relationship between sidewall curvature and elapsed time after unloading. The experimental results [18] were obtained with a similar condition using a grade 2 CP-Ti sheet.

that the curvatures are much smaller in the simulation result than in the experimental result. This is because the strength is larger in the grade 2 sheet than in the grade 1 sheet [2].

Focusing on an integration point near the surface on the die side, the evolutions of relative activities and stress components in the co-rotational frame as a function of time are respectively shown in Figs. 2 and 3. In Fig. 3, x' and y' denote respectively the longitudinal and thickness directions of the sheet. Only the components in the x'-y' plane are shown. When the integration point was subjected to compression in the longitudinal direction due to bending at the die shoulder ($t>2$), pyramidal <a> slip, $\{10\bar{1}2\}$ twinning, basal slip, and prismatic slip were active. Thereafter the loading direction was inverted to tension because of unbending ($t>2.5$). After $\sigma_{x'x'}$ turned to positive, $\{10\bar{1}2\}$ detwinning was active in addition to pyramidal <a> slip and prismatic slip. As the activity of $\{10\bar{1}2\}$ detwinning decreased sharply, the activities of two types of pyramidal <a+c> slip increased. The aforementioned evolution is very similar to that observed during uniaxial reverse loading from compression to tension [3]. Thereafter, during

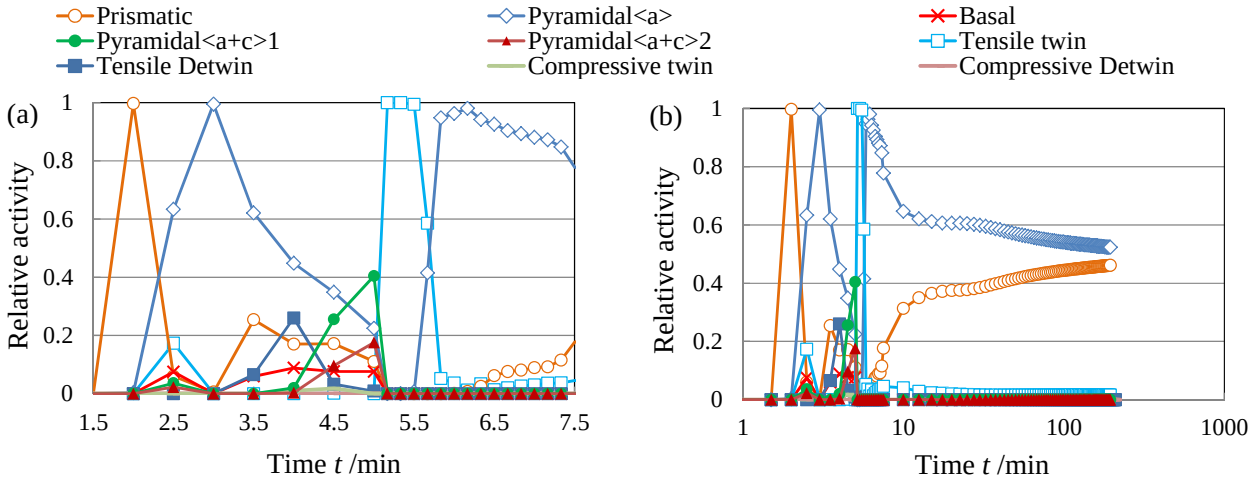

Figure 2. Evolution of relative activities as a function of time at an integration point near the surface on the die side. Evolutions are (a) during forming and unloading and (b) for entire process.

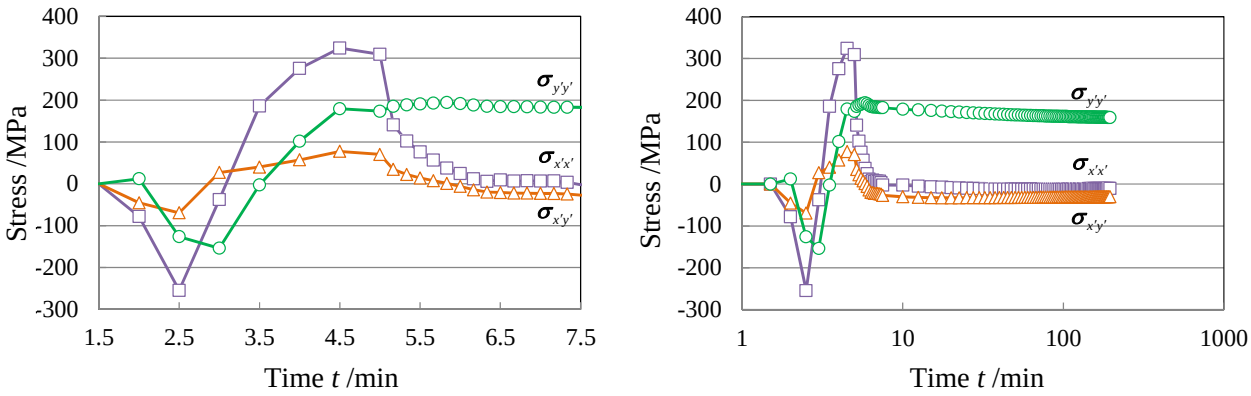

Figure 3. Evolution of stress components in the co-rotational frame as a function of time at an integration point near the surface on the die side. Evolutions are (a) during forming and unloading and (b) for entire process. x' and y' denote respectively the longitudinal and thickness directions of the sheet.

unloading ($5 \le t \le 7.5$), the activity of $\{10\bar{1}2\}$ twinning was dominant initially, but it suddenly decreased and, alternatively, the activity of pyramidal <a> slip rapidly increased. It is presumed that large through-thickness stresses observed after unloading may result from the $\{10\bar{1}2\}$ twinning activity which occurred only near the surface on the die side. The activity of pyramidal <a> slip then decreased gradually, while the activity of prismatic slip gradually increased. $\{10\bar{1}2\}$ twinning was also active to a small extent. These slip and twinning systems were active during unloading because of the heterogeneous stress distribution at the grain level [19]. Further, these three slip and twinning systems kept on activating even after the integration point was macroscopically unloaded from the tools ($t > 7.5$). The slip and twinning activities after unloading would be driven by the residual stresses because non-negligible residual stresses remained after unloading, resulting in the increase in the curvature with the elapsed time. Interestingly, the mechanism of the plastic deformation that occurred after unloading would be very similar to that of creep because the residual stresses remained almost constant or decreased very gradually. This result supports the hypotheses reported in previous studies [11-13,18].

5. Conclusions

In the present study, a crystal-plasticity finite-element method was used to examine the elapsed time-dependent springback of a commercially pure titanium sheet. The simulation results captured the increasing tendency in the amount of springback with the elapsed time observed in experiment fairly well. The simulation results suggested that the increase in the amount of springback after unloading resulted from the slip and twinning activities driven by the residual stresses, and moreover, that the plastic deformation mechanism after unloading was similar to that of creep.

Acknowledgements

This study was partially supported by JSPS KAKENHI Grant numbers 17H03428 and 17K06858 and the Amada Foundation (AF-2015020).

References

[1] Hama, T., Nagao, H., Kobuki, A., Fujimoto, H., Takuda, H., *Mater. Sci. Eng. A*, 620 (2015) 390-398.
[2] Yi, N., Hama, T., Kobuki, A., Fujimoto, H., Takuda, H., *Mater. Sci. Eng. A*, 655 (2016) 70-85.
[3] Hama, T., Kobuki, A., Takuda, H., *Int. J. Plast.*, 91 (2017) 77-108.
[4] Baral, M., Hama, T., Knudsen, E., Korkolis, Y.P., *Int. J. Plast.*, in press.
[5] Ishiki M, Kuwabara T, Yamaguchi M, Maeda Y, Hayashida Y and Itsumi Y, *Trans. Jpn. Soc. Mech. Eng.* **75** (2009) 491-500.
[6] Nixon M.E., Cazacu O., Lebensohn R. A., *Int. J. Plast.* **26** (2010) 516-532.
[7] Mullins, S., Patchett, B.M., *Metall. Trans. A*, 12(1981), 853–863.
[8] Warwick, J.L.W., Jones, N.G., Rahman, K.M., Dye, D., *Acta Mater.*, 60 (2012) 6720–6731.
[9] Chichili, D.R., Ramesh, K.T., Hemker, K.J., *Acta Mater.*, 46 (1998) 1025–1043.
[10] Wang, L., Barabash, R.I., Yang, Y., Bieler, T.R., Crimp, M.A., Eisenlohr, P., Liu, W., Ice, G. E., *Metall. Mater. Trans. A*, 42 (2011) 626–635.
[11] Wang, J.F., Wagoner, R.H., Carden, W.D., Matlock, D.K., Barlat, F., *Int. J. Plast.*, 20 (2014), 2209-2232.
[12] Li, B., McClelland, Z., Horstemeyer, S.J., Aslam, I., Wang, P.T., Horstemeyer, M.F., *Mater. Des.*, 66 (2015) 575-580.
[13] Lim, H., Lee, M.G., Sung, J.H., Kim, J.H., Wagoner, R.H., *Int. J. Plast.*, 28 (2012) 42-59.
[14] Kyuno, T., Tamura, S., *Die & Mould Technol.*, 27 (2012), 28-33 (in Japanese).
[15] Peng, J., Zhou, C.Y., Dai, Q., He, X.-H., *Mater. Sci. Eng. A*, 611 (2014) 123-135.
[16] Whittaker, M., Jones, P., Pleydell-Pearce, C., Rugg, D, Williams, S., *Mater. Sci. Eng. A*, 527 (2010) 6683-6689.

[17] Eipert, I., Sivaswamy, G., Bhattacharya, R., Amir, R., Blackwell, P., *Key Eng. Mater.*, 611-612 (2014), 92-98.
[18] Hama, T., Sakai, T., Fujisaki, Y., Fujimoto, H., Takuda, H., *Procedia Eng.*, 207 (2017), 263-268.
[19] Hama T and Takuda H, *Int. J. Plast.* **27** (2011) 1072–1092.
[20] Hama T, Tanaka Y, Uratani M and Takuda H, *Int. J. Plast.* (2016), 82(2016), 283-304.